Determination of the Branching Ratios for the Reaction of Hot H Atoms with BrCN and ClCN

Brian K. Decker,[†] G. He, I. Tokue,[‡] and R. Glen Macdonald*

Argonne National Laboratory, Department of Chemistry, 9700 South Cass Avenue, Argonne, Illinois 60439

Received: December 11, 2000

The relative rates for the reaction of translationally energetic H atoms with XCN to yield HNC + X, HCN + X, and HX + CN, where X is Br or Cl, have been determined using time- and frequency-resolved absorption spectroscopy. The H atoms were created with an average translational energy of 92 kJ mol^{-1} by the laser photolysis of CH_3SH at a wavelength of 248 nm. The measurements were carried out at a total pressure of several torr. The dominant channel for each reaction system was the production of hydrogen isocyanide, HNC. The relative branching ratios for H + BrCN and H + ClCN were determined to be 0.85/0.13/0.017 and 0.74/0.25/0.01 for the HNC/HCN/HX + CN channels, respectively. The ratio of the total reaction cross sections, σ_{XCN}, was found to be $\sigma_{BrCN}/\sigma_{ClCN} = 0.84$.

I. Introduction

There is an increasing effort, both theoretically[1] and experimentally,[2] to understand the reaction dynamics of systems progressing beyond those composed of three atoms. Reactions occurring among the four or five atom systems denoted by HXCN, where X is a halogen or CN, form an intriguing collection of atoms which can be used to extend our knowledge of polyatomic reaction dynamics beyond the three atom case. The CN radical is closely related to the halogens by its chemical properties such as eletronegativity, and is often referred to as a pseudo-halogen. The dynamics that occur in the HXCN systems should be closely related to that in the three atom systems HYZ, where Y and Z are halogens. There is a great deal of detailed information available about the dynamics of HYZ systems.[3−5] Furthermore, the interpretation of the global dynamical features in HXCN systems may be more easily compared to those observed in HYZ systems because the CN radical may be expected to behave more as a single unit, reducing some of the motions generally accessible in polyatomic systems.

Experimentally, the HXCN reactions have been studied from a variety of different approaches exploring many different facets of the potential energy surfaces (PESs). For example, the portion of the PES dealing with the HX + CN → HCN/HNC + X process has been probed by Smith and co-workers by measuring thermal rate constants[6] and probing the influence of vibrational excitation[7] on the reaction rate constants. Other aspects of the PES have been studied in hot-atom reactions by measuring the product state distribution and translational energy disposal in the CN diatom. De Juan et al.[8] and Johnston and Bersohn[9] initiated the H + ClCN → HCl + CN reaction using photolytically generated H atoms. Using a similar technique, He et al.[10] also studied the H + XCN → HX + CN reactions, where X was Br, Cl, and CN. Another portion of the PES dealing with the H + XCN → HNC/HCN + X channels was probed by Setser and co-workers using infrared chemiluminescence. These workers studied the HCN/HNC product state distribution in the thermal reactions of H + ICN[11] and H + BrCN.[12] A related process, the Cl + HCN(v) → HCl + CN reaction has been investigated in several laboratories using vibrational overtone excitation and thermal or translationally excited Cl atoms. Several different nearly isothermal vibrational energy levels of HCN were excited and the resulting energy disposition into the CN fragment probed.[13−16] In a related work, Macdonald[17] has measured the complete energy disposition into the HNC(0 v_2^1 0) product from the hot H atom reaction H + $(CN)_2$ → HNC + CN.

Theoretically, a great deal of information about the HClCN PES has come from a recent calculation by Harding.[18] This study illustrates the complex nature of PESs dealing with polyatomic reaction systems. The calculations were carried out at the RHF+1+2/cc-pvdz level of theory, with higher level calculations on the properties of the stationary points found on the PES. In all 14 minima and 9 transition states were characterized. The calculated topology of the PES indicated the following: the H + ClCN → HCl + CN reaction occurs through a near linear transition state with a barrier of 91 kJ mol^{-1}. The Cl(H)CN adduct decomposes to only HCN + Cl products. The formation of a cis-ClCNH transition state occurs over a barrier of 46 kJ mol^{-1} and leads to the formation of HNC + Cl products.

The present experiments were carried out to quantify the relative cross sections for energetic H atoms reacting with XCN, where X is Br or Cl, leading to the three possible product channels: HNC + X, HCN + X, and HX + CN. The H atoms were generated by the 248 nm photolysis of CH_3SH in several torr of Ar. The various products, HNC, HCN, HCl, Br, and CN, were monitored by time- and frequency-resolved absorption spectroscopy.

II. Experimental Section

The basic experimental apparatus has been described previously.[19] Briefly, the reaction chamber consisted of a rectangular stainless steel vacuum vessel, which was evacuated by a liquid-

* To whom correspondence should be addressed. E-mail: macdonald@anlchm.chm.anl.gov.

[†] Present address: Physical Sciences Inc., 20 New England Business Center, Andover, MA 01810.

[‡] Also at the Department of Chemistry, Niigata University, Faculty of Science, Niigata 950-21, Japan.

10.1021/jp004465n CCC: $20.00
Published on Web 05/17/2001

nitrogen trapped mechanical pump. Separate vacuum lines supplied the necessary reagent gases at known flow rates. The gases flowed continuously through the apparatus, and their partial pressures were determined from their known flow rates and the reaction chamber pressure.

The photolysis laser was a Lamda Physik Compex 205 excimer laser operating at a wavelength of 248 nm, a power density of approximately 15−20 mJ/cm^2, and a repetition rate of 3−5 Hz. A portion of the excimer laser beam radiation was transmitted through the apparatus and detected by a power meter. This measurement was used to correct the data for the attenuation of the photolysis laser radiation, as described previously.[10]

The HNC, HCN, HCl molecules, and the Br atom were all monitored using time- and/or frequency-resolved absorption spectroscopy. The tunable infrared laser radiation was generated by a Burleigh model 20 single-mode color-center laser. The HNC and HCN molecules were monitored using the fundamental H−NC, ν_1 (100) ← (000) and H−CN ν_3 (001) ← (000) transitions. To ensure that vibrational relaxation was complete on the time scale of the measurements, vibrationally excited levels were also monitored. Similarly, the CN radical was monitored using time- and/or frequency-resolved absorption spectroscopy in the near-infrared using the CN red system, (A $^2\Pi$ ← X $^2\Sigma^+$) (2,0) band near 789 nm. The tunable laser radiation was supplied by an Environmental Optical Sensors external-cavity diode laser. Both laser beams were overlapped using a dichroic mirror, and multipassed through the photolysis region using White cell optics.[19] Both the CN radical and an infrared absorbing species could be simultaneously detected on the same photolysis laser pulse.

Two types of data were recorded, time-resolved and frequency-resolved absorption profiles. The time-resolved studies provided the complete time dependence of the species being monitored while the frequency-resolved profiles provided a detailed measure of the concentration of the species at a specific time following the initiation of the reaction sequence. The frequency resolution of both laser sources was several hundreds times smaller than the 293 K Doppler profile of the species under study. For the time-resolved studies the laser frequency was tuned to the center of an absorption feature, and the signals from 200 to 1000 photolysis laser pulses were averaged using a LeCroy 9410 digital oscilloscope. The initial probe laser intensity, I_o, was recorded using a Stanford model SR-250 boxcar module that was triggered several hundred microseconds prior to firing the photolysis laser. Data collection was controlled by a laboratory computer.

In obtaining time-resolved absorption profiles, there is always some uncertainty in setting the probe laser frequency exactly on the peak of the absorption feature. More accurate concentration measurements are obtained by recording frequency-resolved absorption line profiles at a fixed time following the photolysis laser pulse. To monitor the concentration of both CN and an infrared absorbing species using frequency-resolved absorption profiles, four SR-250 box car modules were used, two for each species, one of which measured the initial light intensity, $I_o(\nu)$ and the other the transmitted intensity, $I(\nu)$, where ν is the frequency of the probe laser radiation. The gate of each boxcar measuring $I(\nu)$ was set at an appropriate time decay for the probed species (determined in the time-resolved measurements) so that vibrationally excited levels had relaxed completely. The frequency-resolved absorption profiles were acquired by incrementing the frequency of each laser in discrete steps, and accumulating an absorption signal for 20−60 photolysis laser pulses until the complete absorption feature had been resolved.

All of the data reported in the present work were obtained at total pressures less than 1.8 Torr. At this pressure, an absorption line of HNC, HCN, and HCl should be well-described by a Doppler profile corresponding to the temperature of the reaction chamber, 293 ± 1 K. To be sure that this was indeed the case, the infrared frequency was monitored by recording high-resolution Etalon peaks from a Burleigh CF-500 Etalon with a free-spectral range, FSR, of 150 MHz. The FSR of the Etalon was calibrated against the reported[20] line positions for the high-resolution absorption spectrum of C_2H_2 near 3.0 μm. The data for the H + BrCN reaction was obtained at a more preliminary stage of the experiment, and the frequency of the infrared laser was not directly monitored during an experiment. However, these experiments were conducted at even lower total pressures, <1.1 Torr, and the influence of pressure broadening should be very small.

For the H + BrCN reaction, only a single CN transition in the A ← X (2,0) band was monitored, and the wavelength scale was calibrated using an evacuated Burleigh WA-20 wavemeter. For the H + ClCN reaction, several closely spaced transitions in the R branch of the F_1 spin−orbit manifold were studied, and the frequencies of the lines were calculated from the spectroscopic data of Cerny et al.[21] The frequency scale calibrated by the wavemeter readings and the CN line positions agreed within ±3% of each other.

The data for the H + BrCN system was not as extensive as that collected for the H + ClCN system. At 293 K, pure BrCN is a white crystalline solid with a vapor pressure of about 60 Torr. Over months of storage in a blacken bulb the BrCN was observed to acquire a yellowish cast, presumably due to the formation of cyanuric bromide. It proved impossible to remove this compound from the glass vacuum system, and it was decided that the experiments with BrCN should be discontinued.

III. Results

A. Analysis. The reaction sequence initiated by the translationally energetic H atoms is given by

$$CH_3SH \xrightarrow{248\ nm} CH_3S + H \quad (1)$$

$$H + XCN \rightarrow HNC + X \quad (2a)$$

$$\rightarrow HCN + X \quad (2b)$$

$$\rightarrow HX + CN \quad (2c)$$

$$CN + CH_3SH \rightarrow HCN + CH_3S/CH_2SH \quad (3a)$$

$$\rightarrow HNC + CH_3S/CH_2SH \quad (3b)$$

if X = Cl

$$Cl + CH_3SH \rightarrow HCl + CH_3S/CH_2SH \quad (4)$$

where X is Cl or Br. All species were lost by diffusion from the photolysis region. The branching ratios, $f_{3a}^{CH_3SH}$ and $f_{3b}^{CH_3SH}$, have been measured recently in this laboratory[22] to be $f_{3a}^{CH_3SH} = 0.81$ and $f_{3b}^{CH_3SH} = 0.19$, respectively. The purpose of the present work was to measure the branching ratios for reaction 2, which requires the measurement of the concentrations of HNC, HCN, and CN, as will be discussed below.

The H atom translational energy distribution from reaction 1 was extrapolated to a photolysis wavelength of 248 nm from the reported[23] Gaussian distribution following the 243.1 nm

photolysis of CH_3SH. The H atoms were calculated to have a mean center-of-mass translational energy, $\bar{E}_H$, of 92 kJ mol^{-1} and a fwhm of 38 kJ $mol.^{-1}$ Although the H atom translational energy was broad it was hoped that the branching ratios defined by $\bar{E}_H$ would be representative of the chemistry occurring in these two systems. Furthermore, if the conditions of the experiment are such that reaction 2 only occurs for H atoms with approximately the initial translational energy distribution, then at least the experimental measurements will be carried out with a known distribution of H atom collision energies, thereby facilitating a comparison between theory and experiment. By comparison with other hot H atom reactions, both experimental[24] and theoretical,[25,26] it is anticipated that the cross sections for reaction 2 should increase with increasing translational energy; thus, the measured branching ratios should be weighted toward those H atoms having the higher translational energy. To this end, the measurements were conducted under conditions where the partial pressure of XCN, P_{XCN}, was low compared to the P_{Ar}, ($P_{Ar}/P_{ClCN} = 28-60$ and $P_{Ar}/P_{BrCN} = 13-6$). This at least ensured that the observed reaction products would more likely arise from H atoms that had the fewest thermalizing collisions with Ar. For the H + ClCN system, the barrier height for reaction 2c has been calculated[18] to be almost equal to $\bar{E}_H$ so that this channel should be very sensitive to the translational energy of the reacting H atoms. As will be seen (section III, part C.) the branching ratio for this process was independent of the P_{Ar}/P_{ClCN} ratio, within the scatter of the measurement, which was interpreted to indicate that the H atoms contributing most to the branching ratio measurements had an energy distribution close to the one initially created. The cross section for thermalization of H atoms with 13 kJ mol^{-1} translational energy by Ar has been measured[27] to be 9×10^{-16} cm^2. As will be discussed in section III,D, the cross section for reaction 2 is about 2×10^{-16} cm^2; hence, the cross section for H atom thermalization was 4.5 times larger than that for reaction.

All the species observed in this work were detected using high-resolution absorption spectroscopy. The absorbance at frequency ν, $A(\nu)$, for a species in quantum state i is given by the Beer−Lambert law as[28]

$$A(\upsilon) = \ln\left(\frac{I_o(\upsilon)}{I(\upsilon)}\right) = 1\sigma(\upsilon)\left([N_i] - \frac{g_i}{g_j}[N_j]\right) \qquad (5)$$

where l is the path length, $\sigma(\nu)$ is the absorption cross section at ν, $[N_k]$ is the concentration of the absorbing species in quantum state k with a degeneracy g_k (The square brackets, [ ], will be used to indicate concentration in molecules cm^{-3}.) The $\sigma(\nu)$ is related to the integrated line strength of the transition, S_{ji}, by the normalized-line shape function, $g(\nu)$, as $\sigma(\nu) = g(\nu)S_{ji}$. At the pressures used in the present experiments, $g(\nu)$ has the familiar Gaussian frequency dependence with the fwhm determined by the translational temperature of the absorber. With slight variations for vibrational or electronic transition moments, the S_{ji} can be calculated from[29]

$$S_{ji} = \frac{8\pi^3}{3hc}\bar{\nu}_{ji}|\langle j|\mu|i\rangle|^2 \frac{A_{ji}}{2J+1} \mathrm{HW} \qquad (6)$$

where c and h have their usual meaning, $\bar{\nu}_{ji}$, is the wavenumber of the transition and $\langle j|\mu|i\rangle$ the transition moment, A_{ji} is the appropriate Hönl-London factor, and HW is the Herman-Wallis factor for the vibrational transitions. Both HCN and HNC are linear triatomic molecules, and as with HCl, the A_{ji} is given by $J + 1$ for an R branch and J for a P branch transition. For the electronic transition of CN, the A_{ji} were calculated according to the formula[30] of Earls's for intermediate coupling between Hund's case a and b.

TABLE 1: Transition Moments for HCN, HCl, HNC and CN

species	$\langle j\|\mu\|i\rangle$ (Debye)	ref
HCN	0.0852 ± 0.0014^a	31, 32, 33
HCl[35]	0.07296 ± 0.00007^b	34
HNC	0.141 ± 0.007^b	35
CN	0.275 ± 0.014^c	36, 37

[a] Average of three investigations. [b] Reported standard deviation in the measurement. [c] Electronic transition moment. Estimated accuracy of the theoretical calculation and within the experimental determination.

The transition moments for the various molecular species monitored in the present work are summarized in Table 1. For HCN, the average of three determinations[31−33] is given in Table 1, and the quoted uncertainty is the standard error. For HCl, only the measurement of Pines[34] is included. For the transient species HNC, the recent experimental measurement[35] is listed, while for CN it was felt that the theoretically[36] calculated value was more appropriate than the experimental[37] value, although the values agree within their quoted uncertainties.

The concentration of the Br atom, [Br], was measured using the $F_2 \leftarrow F_3$ hyperfine level transition of the magnetic dipole allowed Br $^2P_{1/2} \leftarrow {}^2P_{3/2}$ spin−orbit manifold. The expressions for the $\sigma(\nu)$ for the Br atom have been discussed[38,39] recently.

The time dependence of a single rotational level of the ground state for each of the molecular species and the Br atom are shown in Figures 1 and 2 for the H + BrCN system. An initial inversion between the probed ro-vibrational levels for HNC and HCN, according to eq 5, can be seen in Figure 1. Also evident in Figure 2a is the production of the excited Br $^2P_{1/2}$ spin−orbit state, indicated by the slight increase in absorbance following the initial abrupt rise. The Br $^2P_{1/2}$ state is likely produced in the photolysis of BrCN at 248 nm. In any case, except for the rapid removal[22] of CN by CH_3SH, after a suitable delay, the time dependence of each species decayed slowly, indicating that equilibration of excited states had been complete and the species removed by diffusion. In the frequency-scanned measurements, the initial concentration of each species was determined by extrapolating the time dependence back to $t = 0$, using the decay rate of each species measured in the time-resolved absorption experiments under the same experimental conditions.

The determination of the initial [CN] was more difficult because reaction 3 is rapid enough that removal of CN(0, J) occurs on the same time scale as equilibration of CN, for both translational and rotational degrees-of-freedom. The [CN(0)] time profiles were fit to a single-exponential decay and the derived decay rate was used to extrapolate the frequency-resolved scans back to $t = 0$.

B. Branching Ratios for the H + BrCN Reaction. The frequency-resolved scans detecting HNC(000), HCN(000), Br $^2P_{3/2}$, and CN(0), obtained under identical conditions as the time-resolved scans shown in Figures 1 and 2, are presented in Figures 3 and 4. In Figures 3 and 4, the solid lines are nonlinear least-squares fits to the $A(\nu)$ profiles assuming a Gaussian line-shaped function using a program Peak Fit. For the H + BrCN system, the line widths of HNC, HCN, and Br were assumed to be their corresponding Doppler widths for the 293 K temperature of the reaction chamber. For CN, the line width was calculated from a calibration factor determined by a least-squares fit to the wavemeter readings. For CN(0) $R_1(8.5)$, this measured line width was consistent with a temperature of 293 K, with an uncertainty of about 10%.

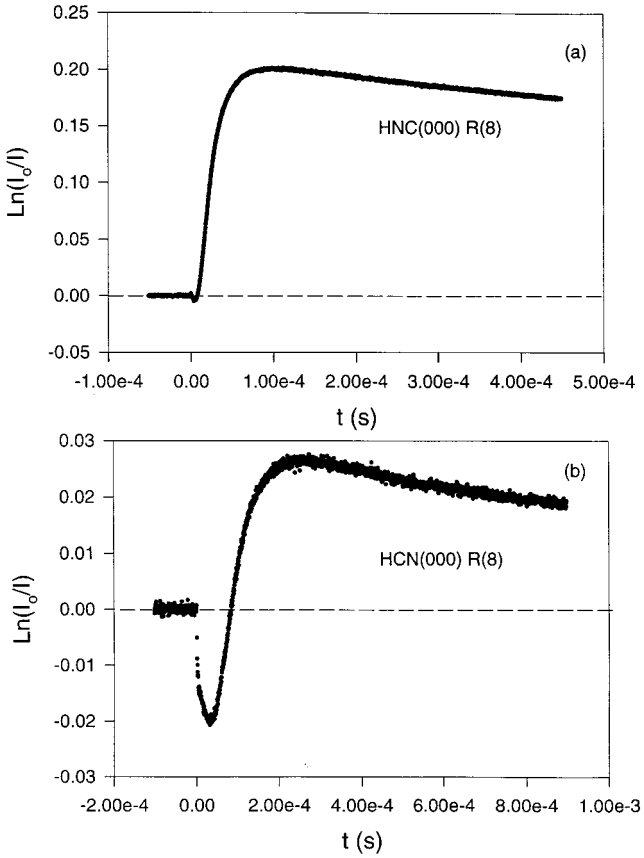

Figure 1. (a) Time-resolved absorption profiles for the HNC(100) ← (000) R(8) transition generated in the H + BrCN reaction. Note the slight initial population inversion, according to eq 5. Vibrational relaxation was complete after about the first 100 μs. The conditions of the experiment were $P_{Ar} = 1.097$, $P_{BrCN} = 0.072$, and $P_{CH_3SH} = 0.033$ Torr at 293 K. (b) Same as panel a except for the HCN(001) ← (000) R(8) transition. Note the much larger population inversion for HCN and the slower vibrational relaxation time period.

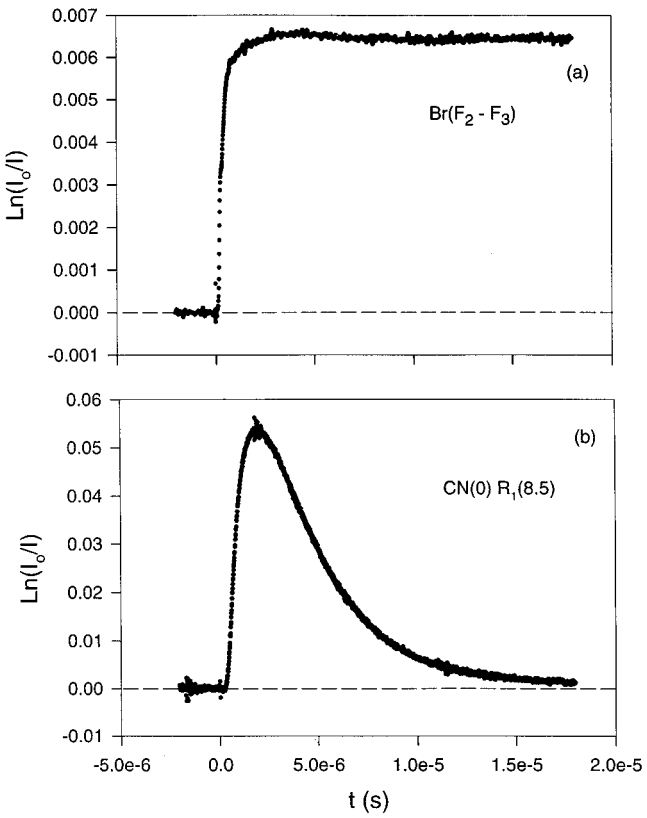

Figure 2. (a) Same experimental conditions as Figure 1 but for the $F_2 \leftarrow F_3$ hyperfine transition of the Br atom generated in the H + BrCN reaction and the photolysis of BrCN. (b) Same as Figure 1a except for the CN ($A^2\Pi \leftarrow X^2\Sigma$) (2,0) R_1(8.5) transition. The CN radical formation was dominated by the photolysis of BrCN. The CN absorption and an infrared absorbing species were followed concurrently.

The absorption cross section[40] of BrCN at 248 nm is quite small, and has been measured to be 1.3×10^{-20} cm.[2] However the production of CN from reaction 2c was also small, and it was found that the observed CN was produced primarily from the photolysis of BrCN. With the CH_3SH flow off, the [CN] was measured by scanning over the CN(0) R_1(8.5) line but at much longer delay times (40 μs compared to 1−2 μs) due to the long rotational relaxation time of the initial highly excited CN radicals[40] ($J_{pk} \approx 50$) created in the photolysis laser pulse. In these experiments, the CN(J) distribution had equilibrated to 293 K. The signal for the much weaker Br atom transitions was too small to accurately determine the [Br]. The absorption cross section[41] for CH_3SH at 248 nm is small (3.0×10^{-19} cm^2), and the attenuation of the photolysis laser beam over the photolysis length was <1% so that the presence or absence of CH_3SH in the gas mixture would not significantly influence the photolysis of BrCN. The [CN] measured in the photolysis experiments was about 30% larger than in the experiments with CH_3SH present. This agreement was considered satisfactory, considering the large correction for the extrapolation back to $t = 0$ (up to a factor of 2, depending on the conditions of the experiment) and the uncertainty in the rotational temperature of CN (set to the observed rotational temperature of CN in the ClCN experiments; see section III,C). In any case, this does indicate that the photolysis of BrCN generated more CN than reaction 2c. The [CN] measured in the photolysis experiments was subtracted from the observed [HNC] and [HCN] to determine the contribution from reaction 2 only.

As a result of the photolysis of BrCN, the f_{2c}^{BrCN} could not be measured in these experiments, but was estimated to be small from the following considerations. The cross sections for reactions (2c) have been measured[10] to be 0.03×10^{-16} and 0.02×10^{-16} cm,[2] for BrCN and ClCN, respectively. This, along with the measurement of f_{2c}^{ClCN}, equal to 0.01 (see section III,C), and the BrCN/ClCN ratio of the total cross sections for reaction 2 equal to 0.84 (see section III,D), were used to estimate that f_{2c}^{BrCN} was approximately 0.017.

Unfortunately, only a few experiments were carried out with BrCN as the reactant, under a restricted set of experimental conditions. A summary of the branching ratio measurements is provided in Table 2. The results are the average of at least two independent measurements of the concentration for each species under the conditions of the experiment. Furthermore, the concentrations determined in the frequency-resolved experiments were in good agreement with those determined in the time-resolved experiments (not reported in Table 2), but with reduced scatter. The contribution of BrCN photolysis to the observed CN is indicated by the ratio of [CN]/[Br], the fourth column in Table 2. If the concentration measurements are self-consistent, then the mass balance expression, ([HNC] + [HCN])/[Br], should be equal to one. As is evident from Table 2, the mass balance expression for this system indicated an excess of Br atoms. The quoted error is a simple error propagation analysis of the observed standard deviations ($\pm 1\sigma$) in the measurement of each concentration.

Besides the uncertainty due to the photolysis of BrCN, there are several other possible explanations for the apparent failure of mass balance. As noted previously, the BrCN was decompos-

TABLE 2: Summary of the Branching Ratio Measurements for the H + BrCN Reaction

P_{Ar} (Torr)	P_{BrCN} (Torr)	P_{CH_3SH} (Torr)	[CN]/[Br][a]	([HNC] + [HCN])/[Br][b]	f_{2a}^{BrCN}	estimated error[c]	f_{2b}^{BrCN}	estimated error
1.097	0.072	0.033	0.20	0.82 ± 0.11	0.90	±0.034	0.097	±0.034
1.090	0.073	0.043	0.19	0.80 ± 0.091	0.84	±0.033	0.16	±0.033
0.633	0.099	0.053	0.10	0.77 ± 0.24	0.88	±0.016	0.12	±0.029
				avg	0.87	±0.028	0.13	±0.032

[a] The observed CN was all attributed to photolysis of BrCN. [b] Measure of mass balance in the experiment. [c] The largest source of uncertainty was the contribution of CN from photolysis ±10%.

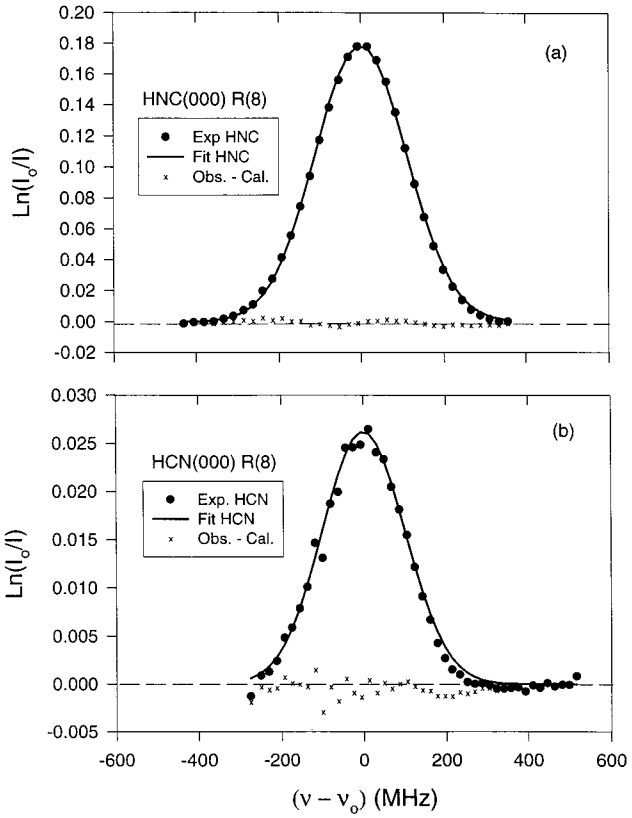

Figure 3. (a) Same as Figure 1a except a frequency-resolved absorption profile for HNC(000) generated in the H + BrCN system acquired after a delay of 200 μs. The solid line is a nonlinear least-squares fit to the experimental points. The fwhm of a Doppler profile for the HNC(000) R(8) transition is 260 MHz. (×) The residuals of the fit. (b) Same as Figure 1b except a frequency-resolved absorption profile for HCN(000) generated in the H + BrCN system acquired after a delay of 300 μs. The fwhm of a Doppler profile for the HCN(000) R(8) transition is 236 MHz at 293 K.

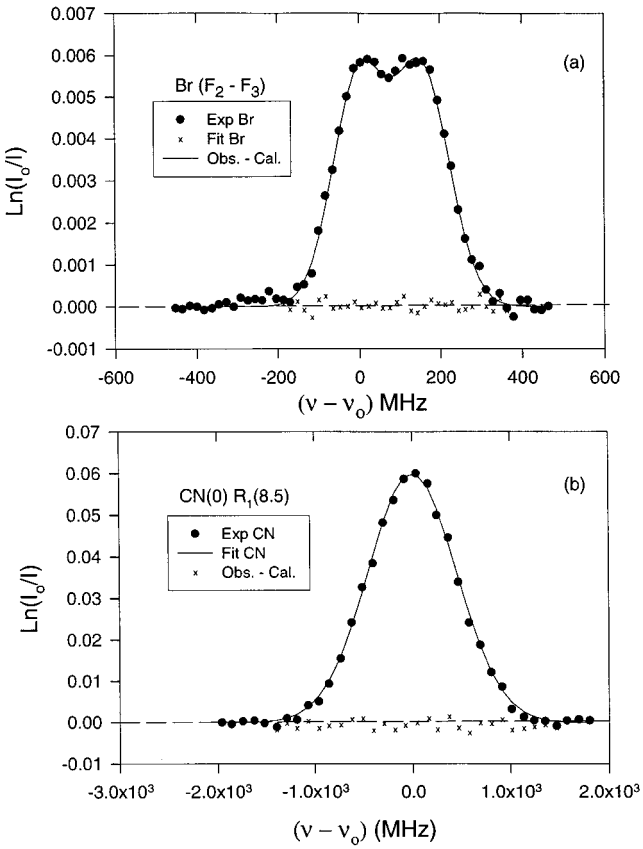

Figure 4. (a) Same as Figure 2a except a frequency-resolved absorption profile for Br atom generated in the H + BrCN system acquired after a delay of 15 μs. The two peaks result for the near equal abundance of Br^{79} and Br^{81} isotopes having the same nuclear spin, $I = {}^3/_2$, but different hyperfine interaction constants. The zero frequency is for the Br^{81} isotope. The fwhm for a Doppler profile of single Br atom isotope is 151 MHz at 293 K. (×) The residuals of the fit. (b) Same as Figure 2(b) except a frequency-resolved absorption profile for CN(0) generated in the H + BrCN system acquired after a delay of 2 μs. The fwhm of a Doppler profile for the CN(0) R_1 (8.5) transition is 924 MHz at 293 K.

ing over the time frame that these experiments were being carried out, and the photolysis of an impurity with a small partial pressure but a large absorption cross section may have been produced atomic Br but not CN. The absorption cross section[42] for Br_2 at 248 nm is smaller than that for BrCN, and cannot be responsible for the generation of excess Br. Alternatively, the CH_3S radical could react with BrCN releasing a Br atom but not CN or HCN; however, no reasonable reaction sequence could be proposed for such a process. Last, the [Br] was calculated using the theoretical LS coupling value for the magnetic transition moment;[38,39] however, the experimental[39] value has been reported to be a factor of 1.073 larger, but with an uncertainty of ±7%, which is comparable to this difference. If the experimentally derived absorption cross section were used instead to determine the [Br], then the measured [Br] would be lowered by 7%, and the mass balance agreement would be one, within the scatter of the measurements. This illustrates an important aspect of measuring branching ratios especially when transient species are involved: the uncertain nature of the transition moments for the species being studied leads to a corresponding uncertainty in the branching ratio measurement.

The results for the branching fractions are summarized in the last four columns of Table 2, with $f_{2a}^{BrCN} = 0.87 \pm 0.028$ and $f_{2b}^{BrCN} = 0.13 \pm 0.032$. Again, the quoted uncertainty is the result of a simple error propagation analysis of the scatter in the measurement of each species contributing to the measurement. As has been mentioned, the estimate of $f_{2c}^{BrCN} \approx 0.017$ can be derived from the ratio of total reaction cross sections for reaction 2 involving BrCN and ClCN (section III,D) and previous studies of reaction 2c. The other branching ratios should be adjusted accordingly, with the final result being $f_{2a}^{BrCN} = 0.85 \pm 0.028$, $f_{2b}^{BrCN} = 0.13 \pm 0.032$, and $f_{2c}^{BrCN} \approx 0.017$.

C. Branching Ratios for the H + ClCN Reaction. Typical frequency-resolved scans of HNC, HCl, HCN, and CN, created in the H + ClCN reaction, are shown in Figures 5 and 6. As in

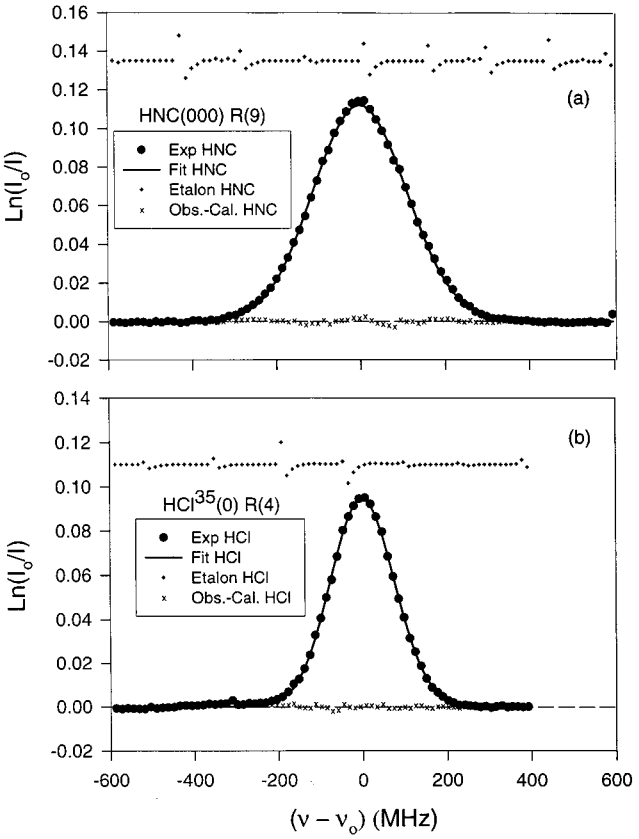

Figure 5. (a) Frequency-resolved absorption profile for the HNC(100) ← (000) R(9) transition generated in the H + ClCN reaction. The signal was acquired after a delay of 200 μs. (+) The signals from a 150 MHz high-resolution Etalon. The solid line is a nonlinear least-squares fit to the experimental points assuming a Gaussian $g(\nu)$ giving a fwhm of 258 ± 4 MHz. (×)The residuals of the fit. The conditions of the experiment were $P_{Ar} = 1.648$, $P_{ClCN} = 0.081$, and $P_{CH_3SH} = 0.030$ Torr. (b) Same as panel a except for the HCl^{35} (1) ← (0) R(4) transition generated in the H + ClCN reaction. The fwhm was measured to be 191 ± 2 MHz corresponding to $T = 325 \pm 7$ K.

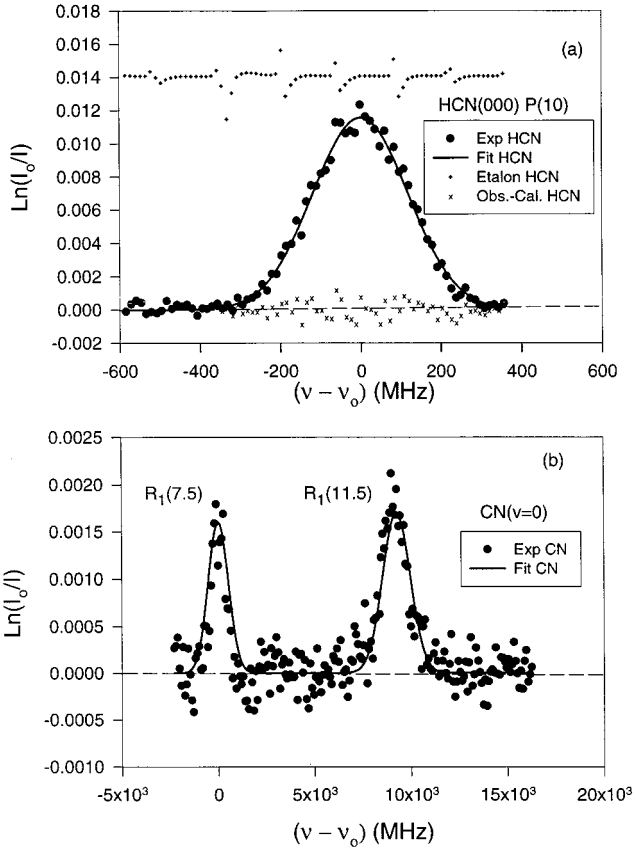

Figure 6. (a) Same as Figure 5a except for the HCN(000) ← (001) P(10) transition generated in the H + ClCN reaction. The fwhm was measured to be 278 ± 7 MHz corresponding to $T = 417 \pm 20$ K. (see text). (b) Same as Figure 5a except for the CN ($A^2\Pi \leftarrow X^2\Sigma$) (2,0) $R_1(7.5)$ and $R_1(11.5)$ transitions generated in the H + ClCN reaction. The fwhms were measured to be 870 ± 120 and 1210 ± 110 MHz, for $R_1(7.5)$ and $R_1(11.5)$, respectively. The ratio of the integrated line shapes for these two transitions corresponds to a rotational temperature of 420 K.

the H + BrCN case, the solid curves are the results of fitting the absorbance profiles to Gaussian-shaped functions. The upper traces in Figures 5a, 5b, and 6a are the Etalon peaks used to calibrate the wavelength scale for the associated infrared scan. Unlike BrCN, there was no detectable CN signal from the photolysis of ClCN at 248 nm so that the branching ratios were determined from the concentration measurements in a straightforward manner, with only a minor correction for the contribution[22] from reactions 3a and 3b.

As is evident from Figure 6b, the signal from CN(0) was small, and only a few rotational transitions could be monitored. This precluded an extensive investigation of the rotational state distribution of [CN] under the experimental conditions. Rather, the initial CN rotational state distribution was estimated from the rotational temperature calculated from the ratio of the area of two rotational transitions in the R_1 branch head region, usually R_1 (11.5) and R_1 (7.5). If the population of the rotational levels were Boltzmann, the [CN] could have been calculated; however, this measurement was further complicated by the fact that the CN translational temperature was apparently not quite the same for each rotational transition. The Doppler width of the lower rotational state was consistent with a translational temperature near 293 K while the higher rotational state Doppler width was consistent with a translational temperature approximately that of the measured rotational temperature. This trend is evident in the line widths of the two CN rotational transitions shown in Figure 6b. As noted in section II, the frequency scale was calibrated from the wavemeter and the calculated peak positions so that the area of each absorption feature was used to determine the population in the two J states. As already alluded to, the determination of [CN] has an additional uncertainty due to the extrapolation of the concentration back to $t = 0$ using the time dependence observed in the time-resolved measurements. The exact value of the CN decay rate in the period of time between the initiation of the reaction and observation is unknown due to the fact that the initial translational ($T_{trans} = 1925$ K) and rotational excitation[10] ($T_{rot} = 950$ K) equilibrate on the same time scale as reaction 3. Fortunately, little [CN] was produced in reaction 2c, and this measurement does not greatly influence the results for the other channels.

For HNC, HCN, and HCl, the frequency-resolved data were collected under conditions where equilibration was expected to be complete, and the translational and internal degrees-of-freedom should be at the 293 K temperature of the reaction chamber. In general, the translational temperatures derived from the measured fwhms of the absorbance profiles were 313 ± 9 K for HNC and 306 ± 18 K for HCl. These measurements were consistent with a translational temperature of 293 K, although the scatter was higher than expected from the calculated uncertainties in the nonlinear least squares parameters and the calibration of the frequency scale. Part of this is due to the fact that the translational temperature determined from the Doppler width depends on the square of the measured fwhm, and a

TABLE 3: Summary of the Branching Ratio Measurements for the H + ClCN Reaction

P_{Ar} (Torr)	P_{ClCN} (Torr)	P_{CH_3SH} (Torr)	$([HNC]_{2a} + [HNC]_{2b} - [CN]_{2c})/[HCl]_2$[a]	f_{2a}^{ClCN}	f_{2b}^{ClCN}	f_{2c}^{ClCN}
1.700	0.028	0.022	1.084	0.7644	0.224	0.012
1.665	0.064	0.022	1.0350	0.754	0.236	00096
1.648	0.081	0.030	0.995	0.749	0.242	0.0092
1.645	0.080	0.048	0.886	0.781	0.208	0.010
1.564	0.075	0.0320	0.957	0.696	0.293	0.011
0.884	0.012	0.012	1.0418	0.714	0.275	0.011
0.801	0.013	0.016	1.000	0.716	0.273	0.011
0.797	0.014	0.015	0.981	0.731	0.258	0.010
	avg:		0.997	0.738	0.251	0.010
	sd:		±0.060	±0.029	±0.029	±0.001

[a] Mass balance in the experiment.

fractional error in the fwhm contributes twice the fractional uncertainty to the measured temperature. For HCN, the translational temperature, as measured from the fwhm of several P branch transitions, was consistently large, 420 ± 50 K. No explanation for this large deviation from the expected value was found. At a pressure of less than 2 Torr of Ar, pressure broadening should be within the scatter of the fwhm measurements. As noted above, the 248 nm absorption cross section for CH_3SH is small, and the temperature rise in the irradiated volume can be calculated to be <1 K. Of course, as was the case for the H + ClCN system, when the population in the absorbing state is calculated from the area of the absorption feature using the integrated line strength, S_{ji}, the results are independent of $g(\nu)$. A summary of the branching ratio measurements for the H + ClCN reaction is given in Table 3. The data reported in Table 3 were derived using the area of the absorption features for all four species and the calculated S_{ji}, and hence, are independent of any assumptions about $g(\nu)$. When the [HCN] was determined using the peak cross section, $\sigma(\nu_o)$, calculated for a 293 K translational temperature, the results were essentially the same as those in Table 3, but with increased scatter.

The results shown for each experiment in Table 3 are the averages of several independent measurements. However, the standard deviations in these measurements were similar to the overall standard deviation in the average branching ratios provided at the bottom of Table 3, and for clarity are not reported. Reaction 4 is fast[43] and all the Cl atoms produced in reaction 2 were converted to HCl; thus, the results can be independently checked for mass balance and self-consistency. In the H + ClCN system, mass balance is expressed as $[HNC]_{2a} + [HCN]_{2b} - [CN]_{2c} = [HCl]_2$, and this is presented as a ratio in the fourth column of Table 3. Despite some scatter in the individual determination of the mass balance, the average mass balance is in good agreement with the expected value of one, and the scatter is consistent with an uncertainty of the order of ±2% for each concentration measurement.

D. Relative Total Cross Section for H + BrCN and H + ClCN. In one experiment, the product yields from the H + BrCN and ClCN reactions were directly compared under identical experiment conditions. After correcting for a slight differences in reagent partial pressures, the ratio of the reaction cross sections was found to be $\sigma_{BrCN}/\sigma_{ClCN} = 0.84$. An estimate of the individual cross sections for reaction 2 follows from the measurement of the cross section for reaction 2c in the HClCN system,[10] the branching ratio measurements in Tables 2 and 3, and the relative total cross section measurements reported in section III,C. The total reaction cross sections were estimated to be 1.7×10^{-16} and 2×10^{-16} cm^2 for the H + BrCN and H + ClCN systems, respectively, within a factor-of-two uncertainty.

TABLE 4: Summary of the Energetics for the H + BrCN and ClCN Systems

reaction system		$\Delta H°$ reaction
reactants	products	(kJ mol^{-1})
H + BrCN[a]	HNC[b] + Br	−98.3 ± 14.5
	HCN[c] + Br	−158.6 ± 10.5
	HBr + CN[d]	−5.4 ± 10.7
H + ClCN[e]	HNC + Cl	−41.1 ± 12.2
	HCN + Cl	−101.4 ± 8.2
	HCl + CN	−13.5 ± 8.4

[a] $\Delta_f H°$ BrCN = 192.8 ± 6.3 kJ mol^{-1} (Case, M. W., Jr., Ed. *NIST-JANF Thermochemical Tables*; AIP: New York, 1998). [b] $\Delta_f H°$ HNC = 192.6 ± 8.2 kJ mol^{-1} (Lee, T. J.; Rendell, A. P. *Chem. Phys. Lett.* **1991**, *177*, 491). [c] $\Delta_f H°$ HCN = 132.3 ± 4.2 kJ mol^{-1} (Berkowitz, J.; Ellison, G. B.; Gutman, D. *J. Phys. Chem.* **1994**, *98*, 2744). [d] $\Delta_f H°$ CN = 432 ± 5 kJ mol^{-1} (Smith, I. W. M. In *The Chemical Dynamics and Kinetics of Small Radicals*, Part I, Liu, K., Wagner, A., Ed.; World Scientific: Singapore, 1995). [e] $\Delta_f H°$ ClCN = 137.3 ± 4 kJ mol^{-1} (*NIST-JANF Thermochemical Tables*).

TABLE 5: Experimental and Theoretical Energy Barriers on the HBrCN and HClCN PES Relevant to Reaction 2

	BrCN[a]		ClCN[b]	
reaction	E_b (kJ mol^{-1})	E_{avail}	E_b	E_{avail}
HNC + X	31 ± 3.3	194	46	137
HCN + X	22 ± 1.7	254	39	197
HX + CN		101	91	109

[a] Experimental determination of the activation energy[12]. [b] Barrier heights from a theoretical calculation with an estimated absolute uncertainty of (12−20) kJ mol^{-1}. [18]

IV. Discussion and Conclusion

The energetics for the H + BrCN and ClCN reactions are summarized in Table 4. The cumulative uncertainties in each $\Delta H°$ are also included in the table. For both systems, all three reaction channels are thermodynamically allowed. For the production of the HNC/HCN + X channels, the H + BrCN system is almost 50% more exothermic than H + ClCN, but because of the relative bond strengths of H−X with respect to X-CN, both systems are thermodynamically similar for the HX + CN channel. In fact, the energy disposition in the abstraction channel is also quite similar in these two systems.[10]

The influence of barrier heights or geometric constraints on the reaction cross sections should be examined because the initial translational energy distribution of the H atoms was broad (fwhm = 38 kJ mol^{-1}), (see section III,A). There are both experimental and theoretical calculations to serve as guides to the appropriate energy barriers in these systems. These values are summarized in Table 5, along with the average energies available to the products for each reaction channel, E_{avail}, defined by

$$E_{avail} = -\Delta H^\circ + \bar{E}_H + RT + E_v^{XCN} \quad (7)$$

where RT accounts for the thermal rotational energy in the linear XCN molecule, and E_v^{XCN} the thermal energy in the low-frequency bending modes of XCN ($E_v^{XCN} \approx 1$ kJ mol^{-1}). On chemical grounds, the barrier heights on the HBrCN PES are expected to be lower than the corresponding barriers on the HClCN PES, and this is borne out by the data presented in Table 5. The barrier heights on the HBrCN PES are lower by about 16 kJ mol^{-1} compared to the same barriers on the HClCN PES. It is likely that the barrier for the abstraction process is also correspondingly lower in the H + BrCN system. Except for reaction 2c in the H + ClCN system, the initial translational energy of the H atoms ($\bar{E}_H = 92$ kJ mol^{-1}) is well above the energy barriers in these systems, and suggests that geometrical constraints play an important role in constraining the size of the reaction cross section.

For HClCN, the theoretical calculations[18] show that there is a deep potential minimum corresponding to an Cl(H)CN intermediate that lies 130 kJ mol^{-1} below the H + ClCN asymptote. By analogy, a similar minimum likely exists in the HBrCN system. The dominant reaction pathway in both the H + BrCN and H + ClCN systems was reaction 2a, the formation of HNC + X. As shown in Table 5, this is not the most exothermic channel, which would be favored if the reaction were dominated by a long-lived X(H)CN complex. The theoretical calculations indicate that the Cl(H)CN complex decomposes to the HCN + Cl product because a high energy ridge separates the HCl + CN product channel from the HCN + Cl channel. In the region of the Cl(H)CN complex, the two channels are separated by a barrier of 117 kJ mol.$^{-1}$ If this ridge were lower than the E_{avail} for the HCl + CN channel, then this decomposition pathway could compete with the one forming HCN + Cl. However, this is not the case, and the present results support the theoretical value for the energy separation between these channels.

The theoretical calculations[18] also show that the transition state leading to the dominant HNC + Cl channel has a cis-ClCNH structure, with an HNC bond angle of 116°. Although the calculations of Harding do not directly explore the collinear attack of the H on the N atom of NCCl, this configuration is expected to be highly repulsive, as found in other calculations[8] and on the related HHCN PES.[44] The HNC + Cl product channel becomes accessible as the HNC angle passes through 180° at the cis−trans HNCCl transition state. The reactive cross section for reaction 2 is likely reduced by geometrical constraints limiting access to the cis-HNCCl transition state.

In previous works,[8−10] the dynamics of reaction 2c was investigated by probing the rotational and translational energy released into the CN fragment, the diatom containing the old bond in the reaction. For this channel, the energy disposition was similar for the two reaction systems,[10] with a large amount of the reaction exothermicity appearing as translational motion, which has been characterized as repulsive energy release.[3] Furthermore, the absolute reaction cross section for reaction 2c was found to be similar for both systems.[10] The measurements reported here for the other channels and the total reaction cross section indicate that this similarity carries over to these other processes as well. As shown in Tables 4 and 5, the E_{avail} for channels 2a and 2b are substantially greater for the H + BrCN reaction; however, the cross sections are quite similar, again indicating that geometrical effects control the size of the reaction cross section.

The intimate chemical properties of Cl and Br, such as electronegativity and covalent size, are fairly similar, and it might be expected that the PESs at the relatively high energies of the H atoms interacting with these two systems are also similar. The one notable difference between the H + BrCN and H + ClCN systems is that the cross section for the production of HCN is a factor of 2 smaller in the H + BrCN system. As noted, this product channel arises from the attack of the H atom on the C atom, in a X(H)CN configuration. The preference for HNC formation in the HBrCN system could be attributed directly to the larger size of the Br atom. First, the larger Br atom simply deflects more potentially reactive H atom trajectories away from the C atom. Second, the cis-XCNH transition state geometry brings the larger Br atom in closer proximity to an H atom approaching the N atom, and prevents the H atom from reaching the C atom after an abortive reactive interaction.

It is interesting to compare branching ratios for the tetra-atomic H + XCN systems to those involving the triatomic H + YZ systems, where Y and Z are halogens. The H + YZ systems have been well-studied, and their detailed dynamics well-characterized.[3,4] For the present comparison, Tamagake and Setser[45] have measured the relative rate constants and branching ratios for thermal H atoms reacting with Y−Z, where Y, Z, are F, Cl, and I. They also discussed the macroscopic branching (relative product channels) in related triatomic systems. A major difference between the tetra-atomic and triatomic systems is the larger bond strengths in the former systems; however, this is compensated for in the present study by the larger translational energy of the H atoms compared to thermal energies. As a result, the total reactive cross sections are similar in the two cases. Unlike the small H + XCN branching fractions into the HX + CN channel, in the H + YZ reactions there is a more democratic partitioning into the HY + Z or HZ + Y pathways. For the interhalogens, the interaction of lowest energy is the one with the H atom approaching the least electronegative halogen. The partitioning into the two product channels is dominated by the height of the appropriate energy barrier for the formation of a particular diatomic channel. This barrier effect is also evident in the H + BrCN system. The dominant channel observed by Arunan et al.[12] using 475 K H atoms was clearly the HCN + Br process not the HNC + Br one observed in the present work although these workers did not directly observed the ground state of either species.

An important dynamical feature of H + YZ reactions is the presence of microscopic-branching collisions. In such encounters, the H atom initially interacts with YZ at the halogen of lower electronegativity but migrates to the other end of the molecule giving the more exothermic product. These trajectories result in a bimodal distribution in the internal state distribution of the diatomic product of the more electronegative halogen.[46,47] If such trajectories occur in the tetra-atomic cases studied in the present work, it is likely that they do not influence the branching ratios. The halogen-like nature of the CN radical falls between F and Cl; however, the theoretical calculations show that the barrier for HCl formation is substantially larger than the barriers for the HCN or HNC formation (Table 5). Thus, the electronegativity trends apparently operative in the H + YZ systems are not present in the tetra-atomic case. The similarity of the branching fractions for reactions producing a triatom + X product vs the HX + CN products indicates that the H atom has an apparent disregard to which halogen atom is bonded to the CN radical, and implies that if microscopic branching collisions are important they do not lead to a significant increase in reactivity for the exothermic channels. More detailed experimental and/or theoretical dynamical studies into the product state distributions of the HNC and HCN fragments are

needed to assess the importance of migratory collisions in the tetra-atomic reaction systems, especially as a function of collision energy.

Acknowledgment. This work was supported by the U.S. Department of Energy, Office of Basic Energy Science, Division of Chemical Sciences, under Contract W-31-109-ENG-38.

References and Notes

(1) Clary, D. C. *Science* **1998**, *279*, 1879.
(2) Casavecchia, P.; Balucani, N.; Volpi, G. G. *Annu. Rev. Phys. Chem.* **1999**, *50*, 347.
(3) Polanyi, J. C. *Science* **1987**, *236*, 680.
(4) Holmes, B. E.; Setser, D. W. *Physical Chemistry of Fast Reactions*; Smith, I. W. M., Ed.: Plenum Press: New York, 1980; Vol. 2, Chapter 2.
(5) Levine, R. D.; Bernstein, R. B. *Molecular Reaction Dynamics and Chemical Reactivity*; Oxford University Press: New York, 1987.
(6) Sims, I. R.; Smith, I. W. M. *J. Chem. Soc., Faraday Trans. 2* **1989**, *85*, 915.
(7) Frost, M. J.; Smith, I. W. M.; Spencer-Smith, R. D. *J. Chem. Soc., Faraday Trans. 2* **1993**, *89*, 2355.
(8) de Juan, J.; Callister, S.; Reisler, H.; Segal, A.; Wittig, C. *J. Chem. Phys.* **1988**, *89*,1977.
(9) Johnson, G. W.; Bersohn, R. *J. Chem. Phys.* **1989**, *90*, 7096.
(10) He, G.; Tokue, I.; Macdonald, R. G. *J. Chem. Phys.* **2000**, *112*, 6689.
(11) Arunan, I.; Setser, D. W. *J. Phys. Chem.* **1991**, *95*, 4190.
(12) Arunan, I.; Manke II, G.; Setser, D. W. *Chem. Phys. Lett.* **1993**, *207*, 81.
(13) Pfeiffer, J. M.; Metz, R. B.; Thoemke, J. D.; Woods, E., III; Crim, F. F. *J. Chem. Phys.* **1996**, *104*, 4490.
(14) Kreher. C.; Theini, R.; Gericke, K.-H. *J. Chem. Phys.* **1996**, *104*, 4481.
(15) Gericke, K.-H.; Kreher, C.; Reinsch, E. A. *J. Chem. Phys.* **1997**, *107*, 567.
(16) Kreher, C.; Rinnenthal, J. L.; Gericke, K.-H. *J. Chem. Phys.* **1998**, *108*, 3154.
(17) Macdonald, R. G. *J. Phys. Chem. A* **2000**, *104*, 10202.
(18) Harding, L. B. *J. Phys. Chem.* **1996**, *100*, 10123.
(19) He. G.; Tokue, I.; Harding, L. B.; Macdonald, R. G. *J. Phys. Chem.* **1998**, *102*, 7653.
(20) Auwera, J. V.; Hurtmans, D.; Carleer, M.; Herman, M. *J. Mol. Spectrosc.* **1993**, *157*, 337.
(21) Cerny, D.; Bacis, G.; Guelachvilli, G.; Roux, F. *J. Mol. Spectrosc.* **1978**, *73*, 154.
(22) Decker, B. K.; Macdonald, R. G. (Manuscript in preparation).
(23) Rogers, L. J.; Ashfold, M. N. R.; Matsumi, Y.; Kawasaki, M.; Whitaker, B. J. *J. Chem. Soc., Faraday Trans.* **1996**, *92*, 5181.
(24) Kessler, K.; Kleinermanns, K. *J. Chem. Phys.* **1992**, *97*, 374.
(25) Bradely, K. S.; Schatz, G. C. *J. Phys. Chem.* **1996**, *100*, 12154.
(26) Bradely, K. S.; Schatz, G. C. *J. Chem. Phys.* **1997**, *106*, 8464.
(27) Park, J.; Schafer, N.; Bersohn, R. *J. Chem. Phys.* **1989**, *91*, 7861.
(28) Kroto, H. W. *Molecular Rotational Spectra*; Dover: New York; p 69.
(29) Smith, M. A. H.; Rinsland, C. P.; Fridovich, B. *Molecular Spectroscopy: Modern Research*; Rao, K. N., Ed.; Academic Press: Orlando, 1985.
(30) Earls, L. T. *Phys. Rev.* **1935**, *48*, 423.
(31) Smith, I. W. M. *J. Chem. Soc., Faraday Trans.* **1981**, *77*, 2357.
(32) Smith, M. A. H.; Harvey, G. A.; Pellet, G. L.Goldman, A.; Richardson, D. J. *J. Mol. Spectrosc.* **1984**, *105*, 105.
(33) Varghese, P. L.; Hanson, R. K. *J. Quantum Radiat. Transfer* **1984**, *31*, 545.
(34) Pine, A. S.; Fried, A.; Elkins, J. W. *J. Mol. Spectrosc.* **1985**, *109*, 30.
(35) He, G.; Macdonald, R. G. *Chem. Phys. Lett.* **1999**, *301*, 175.
(36) Knowles, P. J.; Werner, H.-J.; Hay, P. J.; Cartwright, D. C. *J. Chem. Phys.* **1988**, *89*, 7334.
(37) He, G.; Tokue, I.; Macdonald, R. G. *J. Chem. Phys.* **1998**, *109*, 6312.
(38) Morter, C. L.; Farhat, S. K.; Adamson, J. D.; Glass, G. P.; Curl, R. F. *J. Phys. Chem.* **1994**, *98*, 7029.
(39) He, G.; Seth, M.; Tokue, I.; Macdonald, R. G. *J. Chem. Phys.* **1999**, *110*, 7821.
(40) Russell, J. A.; McLaren, I. A.; Jackson, W. M.; Halpern, J. A. *J. Phys. Chem.* **1987**, *91*, 3248.
(41) Barone, S. B.; Turnipseed, A. A.; Gierzak, T.; Ravishankara, A. R. *J. Phys. Chem.* **1994**, *98*, 11969.
(42) Wen. W. Y.; Noyes, R. M. *J. Phys. Chem.* **1972**, *76*, 1017.
(43) Nicovich, J. M.; Wang, S.; Wine, P. H. *Int. J. Chem. Kinet.* **1995**, *27*, 359.
(44) ter Horst, M. A.; Schatz, G. C.; Harding, L. B. *J. Chem. Phys.* **1996**, *105*, 558.
(45) Tamagake, K.; Setser, D. W. *J. Phys. Chem.* **1979**, *83*, 1007.
(46) Polanyi, J. C.; Skrlac, W. J. *J. Chem. Phys.* **1977**, *23*, 167.
(47) Tamagake, K.; Setser, D. W. *J. Phys. Chem.* **1979**, *83*, 1000.